Published in final edited form as:
Nat Chem Biol. 2011 April ; 7(4): 228–235. doi:10.1038/nchembio.539.

Uptake of unnatural trehalose analogs as a reporter for *Mycobacterium tuberculosis*

Keriann M Backus[1,2], **Helena I Boshoff**[2], **Conor S Barry**[1], **Omar Boutureira**[1], **Mitul K Patel**[1], **François D'Hooge**[1], **Seung Seo Lee**[1], **Laura E Via**[2], **Kapil Tahlan**[2], **Clifton E Barry III**[2,★], and **Benjamin G Davis**[1,★]

[1]Department of Chemistry, University of Oxford, Chemistry Research Laboratory, Oxford, UK

[2]Tuberculosis Research Section, Laboratory of Clinical Infectious Diseases, US National Institute of Allergy and Infectious Disease, Bethesda, Maryland, USA

Abstract

The detection of tuberculosis currently relies upon insensitive and unspecific techniques; newer diagnostics would ideally co-opt specific bacterial processes to provide real-time readouts. The trehalose mycolyltransesterase enzymes (antigens 85A, 85B and 85C (Ag85A, Ag85B, Ag85C)) serve as essential mediators of cell envelope function and biogenesis in *Mycobacterium tuberculosis*. Through the construction of a systematically varied sugar library, we show here that Ag85 enzymes have exceptionally broad substrate specificity. This allowed exogenously added synthetic probes to be specifically incorporated into *M. tuberculosis* growing *in vitro* and within macrophages. Even bulky substituents, such as a fluorescein-containing trehalose probe (FITC-trehalose), were incorporated by growing bacilli, thereby producing fluorescent bacteria; microscopy revealed selective labeling of poles and membrane. Addition of FITC-trehalose to *M. tuberculosis*–infected macrophages allowed selective, sensitive detection of *M. tuberculosis* within infected mammalian macrophages. These studies suggest that analogs of trehalose may prove useful as probes of function and for other imaging modalities.

Tuberculosis is an infection that has plagued mankind for millennia. It remains a leading cause of death worldwide and was implicated in an estimated 1.6 million fatalities in 2005 (ref. 1). A substantial obstacle to the development of new diagnostics, drugs and vaccines is the lack of tuberculosis-specific probes that can be used to rapidly assess infection and monitor response to treatment[2]. The cell envelope of *M. tuberculosis* poses a significant permeability barrier that contributes to the intrinsic difficulties in eradicating this disease as

★Correspondence and requests for materials should be addressed to C.E.B. or B.G.D. ben.davis@chem.ox.ac.uk or cbarry@niaid.nih.gov.

Author contributions

K.M.B., H.I.B., C.S.B., L.E.V., C.E.B. and B.G.D. designed experiments. K.M.B., O.B., M.K.P., F.D. and S.S.L. synthesized compounds. K.M.B., K.T. and H.I.B. performed uptake experiments. C.S.B. and K.M.B. performed substrate screens. K.M.B., H.I.B., C.S.B., C.E.B. and B.G.D. analyzed results. K.M.B., C.E.B. and B.G.D. wrote the paper.

Competing financial interests

The authors declare competing financial interests: details accompany the full-text HTML version of the paper at http://www.nature.com/naturechemicalbiology/.

Additional information

Supplementary information and chemical compound information is available online at http://www.nature.com/naturechemicalbiology/. Reprints and permissions information is available online at http://npg.nature.com/reprintsandpermissions/.

it effectively precludes entry of most substances (including potential drugs and probes) to the bacterial cytoplasm[3].

The nonmammalian, disaccharide sugar trehalose (**1**, Fig. 1a) is synthesized by *M. tuberculosis* through three independent pathways, and genetic knockouts of any of these three pathways results in either nonviable *M. tuberculosis* or organisms showing growth defects[4,5]. Because of this essentiality, targeting the trehalose pathway may be an important approach to tuberculosis drug development. Trehalose is found in the outer portion of the mycobacterial cell envelope along with the glycolipids trehalose dimycolate (TDM, Fig. 1a) and trehalose monomycolate (TMM, Fig. 1a)[6]. TMM and TDM are important glycolipids for *M. tuberculosis*, capable of inducing granuloma formation in the absence of infection[7]. Mycolic acids are long (C60–C90), cyclopropanated lipids found in the cell wall of *M. tuberculosis*, which are important for bacterial outer membrane structure, virulence and persistence within the host[8]. Trehalose is anchored into the mycobacterial cell wall as mono- (TMM) or di- (TDM) mycolates by the action of the extracellular proteins Ag85A, Ag85B and Ag85C. Although these proteins were long known to immunologists by virtue of their immunogenicity, their enzymatic activity was first described in 1982 as the active fraction of a cell-free extract from *Mycobacterium smegmatis* that was capable of synthesizing TDM[9]. Ag85A, Ag85B and Ag85C are the most abundantly secreted *M. tuberculosis* proteins *in vitro*, accounting for as much as 41% of the total protein in culture supernatant[10]. Individual knockouts of the genes that code for single members of the Ag85 family have significant effects on total cellular mycolic acid content[11]; triple knockouts of the *ag85ABC* genes have not been reported in *M. tuberculosis*, presumably because they are not viable. Ag85 isoforms all catalyze the reversible transesterification reaction between two units of TMM, generating TDM and free trehalose (Fig. 1a); the reverse reaction also allows for direct esterification of trehalose. Ag85 can also covalently introduce mycolates into arabinogalactan to form the base polymer of the cell wall[11,12].

Ag85A, Ag85B and Ag85C share high sequence and structural homology[13–15], characterized by an α,β-hydrolase fold and a hydrophobic fibronectin-binding domain. Their active sites are highly conserved, featuring a histidine, aspartic acid or glutamic acid and serine catalytic triad, a hydrophobic tunnel for the lipids and two trehalose binding sites (Fig. 1b). These characteristics suggest a transesterification mechanism analogous to that of serine hydrolases, in which the formation of a covalent serine-mycolic acid enzyme intermediate is followed by attack from the 6-hydroxyl of trehalose[13].

Structural analysis (Fig. 1c) of trehalose bound to Ag85B suggested positions (C-4′ and C-2) on trehalose that were directed outward toward solvent and that might tolerate substitutions and yet retain activity as substrates for Ag85. Trehalose itself has been demonstrated to be a substrate of Ag85 (refs. 9,16) and its uptake and use by *M. smegmatis* has been observed[5,17]. Although early observations[18] suggest the uptake of trehalose uptake into whole cells of *M. tuberculosis*, this has not been fully investigated, and the corresponding activities of trehalose analogs have not been explored.

We show here not only that Ag85A, Ag85B and Ag85C are sufficiently promiscuous to process a variety of trehalose analogs with good efficiency but that trehalose and trehalose-probe analogs are also efficiently anchored to *M. tuberculosis*. We have exploited this substrate tolerance by designing fluorescent trehalose probes that are processed by Ag85 and that allow fluorescent labeling of *M. tuberculosis* in a selective manner. Our findings arm tuberculosis biologists with the first fluorescent small-molecule probe to label *M. tuberculosis* not only in culture but also in infected macrophages.

RESULTS

Exogenous trehalose is incorporated into TMM and TDM

We first sought to conclusively demonstrate that trehalose is taken up by live cells of *M. tuberculosis in vitro* (Fig. 2). Unlike its fast-growing relative *M. smegmatis*, which has 28 sugar transporters, the genome of *M. tuberculosis* encodes only five sugar permeases, suggesting that extracellular trehalose might not be efficiently taken up by mycobacteria[17]. Extracellular incorporation of trehalose into TMM or TDM, on the other hand, would not require transport across the cell envelope. Using comparative radioprobes ^{14}C-acetate, ^{14}C-glycerol, ^{14}C-glucose and ^{14}C-trehalose, we measured uptake in pathogenic *M. tuberculosis* over 2 and 24 h time periods (Figs. 2a and Supplementary Results, Supplementary Fig. 1). Trehalose uptake was significant, and the strongest band labeled by ^{14}C-trehalose comigrated with a band labeled by ^{14}C-acetate and comigrated with cold TMM. ^{14}C-trehalose also labeled a band that comigrated with TDM, although not labeled to the same extent as TMM. To confirm that these bands were TMM and TDM, we also labeled cells after treatment with isoniazid (INH), which inhibits mycolic acid biosynthesis and therefore blocks production of both TMM and TDM[19]. INH effectively blocks biosynthesis of these two bands (see Fig. 2c (lane iii)). Together these results demonstrated that trehalose is taken up by the bacteria and incorporated into TDM and TMM by *M. tuberculosis in vitro* (Fig. 2c and Supplementary Fig. 2).

M. tuberculosis is thought to infect the alveolar macrophages that line the lung epithelium; macrophage uptake therefore represents an additional permeability hurdle that separates any potential probe from *M. tuberculosis*[20]. We therefore labeled *M. tuberculosis*–infected J774 cells (a mouse macrophage-like cell line) and separately analyzed the macrophage supernatant, crude lysate and insoluble fractions (Fig. 2b) of both infected and uninfected cells. Not only did ^{14}C-trehalose successfully penetrate and internalize into mouse macrophages, it was also subsequently taken up by *M. tuberculosis* growing within these cells, thereby validating the potential of trehalose probes *in vivo*.

Design and synthesis of a trehalose analog library

To fully explore the potential of trehalose analogs as possible selective probes of *M. tuberculosis*, we designed and synthesized (see Supplementary Methods for details) a panel of compounds (Fig. 3) that would allow us to evaluate the substrate tolerance of Ag85 isoforms. This library of trehalose analogs featured systematic modifications at each position to explore the enzyme active site in detail. Such trehalose derivatives present unique synthetic challenges: creating the link between the two glucose units requires that two stereogenic centers with challenging configuration[21] be established simultaneously, and the symmetry of the trehalose scaffold itself necessitates potentially complex asymmetric modifications. Elegant intramolecular, aglycone-tethered glycosylation strategies[22] have allowed access to some C-2 modifications and stereocontrol, yielding the α,α(1,1)-anomeric configuration found in natural trehalose, but are limited in their scope of diversification. Most previous modifications of the trehalose scaffold, including previously designed inhibitors of Ag85, have focused only on modifications at C-6 and C-4 (refs. 23–25).

Our trehalose-probe library was synthesized using complementary strategies for (i) directly creating the 1,1-linkage in trehalose and (ii) precise trehalose scaffold alteration (Supplementary Scheme 1), allowing access to analogs **2**–**22** bearing alterations in both the functional groups and in the stereochemical configurations found at all positions C-1, C-2, C-3, C-4 and C-6 in trehalose. Functional groups were chosen for incorporation that might later be useful in the design of imaging probes such as fluorine (2-F, 3-F, 4-F, 6-F

derivatives) for potential use in ^{18}F-PET and amines for late-stage attachment of chromophores, radiolabels and fluorophores.

1,1-linkage formation was accomplished in three ways: (i) ketoside formation[26,27], (ii) dehydrative glycosylation[28] and (iii) chemoenzymatically[29]. Full characterization of the synthesized probes included unambiguous assignment of stereochemistry using NMR (NOE and H-1 coupling constants). Methyl ketosides and exo-glycals proved to be excellent reagents for α,α-selective synthesis of asymmetric trehalose from a wide range of modified coupling partners, including derivatives of glucose, 2-deoxy-2-fluoro-glucose, 3-deoxy-3-fluoro-glucose and 2-*N*-carbobenzyloxyamino-glucose, yielding trehalose analogs **2**–**7** in good overall yields (30–90%) after deprotection (see Supplementary Methods). Symmetric dideoxy **10**, diiodo **12** and difluoro **13**, **14** trehalose analogs were accessed through dehydrative dimerization reactions[28]. 2-Deoxy-2-fluoro-trehalose **22** was synthesized using a multistep enzymatic route. Finally, trehalose-scaffold modifications used regioselective protecting group manipulation[25] to allow selective asymmetric access and replacement of hydroxyl groups at positions 4 and 6 (see Supplementary Methods for full details).

Together these synthetic routes allowed ready access to trehalose analogs **2**–**22** containing modifications such as 1-methyl **2**–**9**, 2-fluoro **3**, **5**, **13**, **14** and **22**, 2-iodo **12**, 2-deoxy **10** and **11**, 3-fluoro **6**, 4-fluoro **21**, 6-fluoro **20**, 6-bromo **19**, 6-phosphate **15**–**17**, 6-azido **18** and even stereoisomers **4**, **5** and **11** and allowed access to intermediates such as 2-amino-trehalose **7** onto which imaging labels fluorescein (in **9**), fluorobenzyl (in **8**) and even quantum dots (in trehalose-QD, see Supplementary Methods) could be coupled.

A new assay of trehalose processing

The complete substrate specificity and a full kinetic analysis of the Ag85 enzymes has not previously been demonstrated, presumably because of the difficult nature of the radiochemical assay using natural substrates. Heterogeneity in the mycolic fatty acid chain length (C30–C90) and low solubility of both substrates and products in aqueous medium have complicated prior assays. The widely used ^{14}C-trehalose radioassay[16] monitors ^{14}C-trehalose radiolabel incorporation into TDM and TMM yielding, at best, approximate $k_{cat(app)}$ values; such assays have suggested that Ag85B has a lower (~20%) activity than Ag85A and Ag85C[16].

Mass spectrometric analysis[30] provided a rapid means to screen trehalose analogs **1**–**24** as substrates of all Ag85 isoforms (Table 1). Ag85A, Ag85B and Ag85C were prepared and purified as previously described[16] (see Supplementary Methods and Supplementary Figs. 3–8). We designed an assay (see Supplementary Methods) based on the use of precise, homogeneous mono and dihexanoyl trehalose substrates, which proved to be water soluble and readily turned over by Ag85, allowing the development of a broad Ag85 substrate screen (Supplementary Scheme 2). A calibrated green-amber-red[30] screen for catalysis of transfer of the acyl chain from natural trehalose to unnatural trehalose-analog (trehalose*) using these pure synthetic substrates allowed determination of relative reactivity ratios of trehalose*/trehalose (Table 1). Notably, this screen revealed a strong selectivity for trehalose-like disaccharides over monosaccharides such as D-glucose (**23**) but a striking plasticity for all tested trehalose analogs. Modifications on every position of the sugar scaffold were tolerated, including even C-1 methyl groups at the crowded anomeric linkages in **2**–**9**, positive charges, such as in the 2-amino-trehalose **7** and even stereochemically ‘incorrect’ 2,2′-di-fluoro-αβ-mannotrehalose **14**. Even a previously reported inhibitor[16], 6-azido-trehalose **18**, and putative tetrahedral intermediate analogs, such as trehalose-6-phosphate **16**, were also processed.

Prior reports of **18** as an inhibitor (albeit a weak one with a reported minimum inhibitory concentration (MIC) against a related mycobacterial species of 200 μg ml^{-1})[16] prompted us to examine the possibility that these analogs also induced growth inhibition; MIC analysis was therefore carried out on key representative compounds (Table 1). Among these only 2,2′-dideoxy-lyxo-trehalose **11**, which was not a substrate for any of the three Ag85 isoforms, showed an inhibitory effect (MIC 100 μg ml^{-1}). C-6–modified compounds that were processed well by Ag85 inhibited growth only at high concentrations (MIC 100–200 μg ml^{-1}). Notably, no growth inhibition with FITC-trehalose was noted either *in vitro* or in infected macrophages (see Supplementary Fig. 9).

FITC-trehalose specifically labels *M. tuberculosis in vitro*

Next we explored the uptake of fluorescent probes in growing cells of *M. tuberculosis* (Fig. 4a, Supplementary Fig. 11). The pathogenic *M. tuberculosis* strain H37Rv was grown for 24 h in the presence of FITC-trehalose and then washed to remove unbound dye. A significant increase in fluorescence over time was observed in bacteria exposed to FITC-trehalose, relative to the autofluorescence of the control bacteria and relative to heat-killed *M. tuberculosis* that had been treated with FITC-trehalose (Supplementary Figs. 10–12). Heat-killed *M. tuberculosis* form large aggregates that are particularly difficult to wash adequately, perhaps contributing to the relatively high background observed in these organisms. To demonstrate that incorporation was specific, we also monitored incorporation of FITC-glucose into live cells of *M. tuberculosis* and found significantly less incorporation of label into cells (Supplementary Fig. 10b), consistent with the poor efficiency of glucose as a substrate for the Ag85 enzymes (and the unlikely uptake of this probe into the cell by glucose-specific transporters). To demonstrate that this incorporation was dependent upon Ag85, we obtained a mutant in Ag85C that has been previously reported to have 40% less mycolic acid incorporation into the mycobacterial cell wall[11]. This mutant incorporated approximately 30% less FITC-trehalose than did wild type (Supplementary Fig. 10a), supporting our proposed mechanism of anchoring of FITC-trehalose through Ag85-mediated incorporation of mycolic acids. To unambiguously establish that FITC-trehalose was localizing to cells by virtue of being esterified with mycolic acids, we simultaneously labeled cells with both FITC-trehalose and ^{14}C-acetate and isolated individual fluorescent spots by preparative TLC (Fig. 2c). We did not make any attempt to characterize the other less polar spots of low abundance that also apparently incorporated FITC-trehalose, although these might reasonably be supposed to be other trehalosecontaining glycolipids found within the mycobacterial cell wall[31,32]. Saponification of these spots and subsequent methylation and TLC revealed that the strongly fluorescent spots carrying FITC-trehalose were associated with lipids comigrating with the characteristic triplet pattern of the three classes of mycolic acids (alpha, methoxy and keto) (Fig. 2d). Finally, to establish specificity of labeling, we also exposed three other organisms commonly found in the human lung to FITC-trehalose: *Staphylococcus aureus*, *Haemophilus influenzae* and *Pseudomonas aeruginosa*. None of these organisms were found to show appreciable labeling with FITC-trehalose (Supplementary Fig. 10b).

The value of FITC-trehalose as a probe was demonstrated by the clear patterns of differential accumulation within live *M. tuberculosis* (Fig. 4a–**d**, Supplementary Figs. 11–13). For example, confocal fluorescence microscopy of H37Rv–*M. tuberculosis* expressing a red fluorescent protein (RFP, here mCherry, carried by a PMV261 plasmid) revealed higher levels of green fluorescence from FITC-trehalose incorporation at outer membranes and, in particular, at the bacterial poles, and less in mid sections (where the RFP localizes, Fig. 4c, Supplementary Figs. 11–12). This specific polar localization was confirmed by microscopic sections along the Z-axis (Z-stacks, Supplementary Fig. 11) and by statistical analysis of mean fluorescence ($P < 0.0001$, Fig. 4d). These observations are not only consistent with the

mode of action proposed for these trehalose analogs but also suggest higher Ag85 activities at the poles that are consistent with a polar growth model.

FITC-trehalose labels *M. tuberculosis* macrophages

We next tested the ability of these probes to selectively label *M. tuberculosis* in mammalian cells during infection. Treatment of *M. tuberculosis*–infected macrophages with FITC-trehalose (Fig. 4e–n) demonstrated that the probe was internalized into macrophages with subsequent labeling of the bacteria. The specificity of the label for *M. tuberculosis* was demonstrated by colocalization of staining with an *M. tuberculosis*–specific antibody (ab905, Supplementary Fig. 13), use of an alternative labeling strategy (Supplementary Fig. 14) and failure to observe labeling with FITC-glucose (Supplementary Fig. 15). Labeling of the intra-macrophage bacteria was also effectively abolished by competing administration of high concentrations (10–100 mM) of trehalose (Supplementary Fig. 16).

In contrast to the fairly uniform labeling of bacilli observed *in vitro*, bacterial labeling *in vivo* was not uniform, either between cells or within a cell. We observed the same polar localization of label in *in vivo*–grown cells that was seen in the *in vitro* cells; however, some bacterial cells appeared to incorporate no label at all. By incorporating a constitutively expressed RFP in the infecting bacilli (either integratively transformed *Mycobacterium bovis* BCG expressing the DsRed1 gene[33] or the H37Rv–*M. tuberculosis* mCherry variant (see above), for comparison) we observed that even mycobacterial cells within a single macrophage showed very different labeling intensities (Fig. 4h–k). We speculated that this differential FITC-trehalose labeling might be relevant to the growth status of a particular bacterium within the cell, reflective of the maturation status of the endosomal compartment within which they were located. TDM has been shown to inhibit fusion between vesicles[34] and is potentially responsible for the inhibition of phagosomal acidification by *M. tuberculosis*[35]. To test this hypothesis, mouse bone marrow macrophages (BMMs) were infected with RFP-expressing H37Rv and treated with FITC-trehalose, with or without activation by interferon-γ (IFN-γ). Colocalization studies were undertaken between the H37Rv and markers discriminating between endosomes, phagosomes and lysosomes, including the early endosome–associated antigen (EEA-1)[36], Rab5 (ref. 36), Rab14 (ref. 37), procathepsin D[38] and the lysosomal associated membrane protein (LAMP-1 (ref. 39)). Colocalization was then assessed by confocal microscopy between these markers and the entire bacterial population as well as the highly FITC-trehalose–labeled subpopulation. As expected, low colocalization was observed both under activated and unactivated conditions for EEA-1 (Supplementary Fig. 18). Consistent with previous reports of accumulation of Rab5 in the mycobacterial phagosome, we observed consistent colocalization of this marker (Supplementary Fig. 19) with both total population of bacteria and high FITC-trehalose–labeled bacilli in unactivated macrophages.

Upon IFN-γ activation, however, Rab5 colocalization was found to be less for highly FITC-trehalose–labeled *M. tuberculosis* than the bulk bacterial population (Supplementary Fig. 19). Colocalization between Rab14 and FITC-trehalose–labeled *M. tuberculosis* compared to the total population of bacteria was comparable for both unactivated and IFN-γ–treated macrophages (Supplementary Fig. 20). In contrast, procathepsin D, cleavage of which is a marker of phagosomal maturation and phago-lysosome fusion, was increased in colocalization with FITC-trehalose–positive *M. tuberculosis* relative to the whole population (Supplementary Fig. 21). LAMP-1 was also found to colocalize to a lesser degree with highly FITCtrehalose– positive bacteria (Fig. 4h–k) than the population average, particularly upon IFN-γ activation (Fig. 4k–n). Together these data are consistent with the hypothesis that *M. tuberculosis* that poorly incorporate FITC-trehalose tend to be localized to Rab5-containing phagosomes that have more fully matured toward degradative lysosomes. The corollary is that those with high Ag85-activity that incorporate FITC-trehalose well and will

therefore readily generate TDM are associated with less-developed phagosomes, perhaps through TDM-associated inhibitory mechanisms[34,35].

DISCUSSION

Despite decades of investigation for both their immunologic and enzymatic activities, the Ag85 enzymes remain poorly understood. Little is known about the range of their substrates and the reason for their apparent functional redundancy in *M. tuberculosis*. The uptake of ^{14}C-trehalose into *M. tuberculosis in vitro* as well as into infected macrophages suggested that trehalose analogs may be useful in designing new probes of tuberculosis pathogenesis. Using a new Ag85 substrate assay, we have found that Ag85A, Ag85B and Ag85C will tolerate surprisingly extensive modifications on the trehalose scaffold, processing many disaccharides well (but not monosaccharides).

The discovery of the breadth of substrates processed by Ag85 isoforms could have important implications for the biological roles of these enzymes. The enzyme-specific differences in substrate tolerance observed imply an unappreciated subtlety in the active site architecture of these enzymes. Numerous glycolipids within *M. tuberculosis* contain a trehalose core, including TDM, TMM, pentaacyl trehalose, triacyl trehalose and sulfolipid-1 (SL-1); little is known about the final acylation steps of pentaacyl trehalose, triacyl trehalose and SL-1, and the enzymes of the Ag85 complex have been postulated to be involved in the lipidation of these compounds[31,32]. The substrate plasticity, particularly at the C-2 position, may also have implications in the final acylation steps of sulfolipid-1, which are unknown, but have been postulated to potentially occur via Ag85 (ref. 31). Glucose and arabinose, both of which have been proposed as native enzyme substrates, are processed, albeit poorly relative to trehalose dissacharides[11,12,40]. The ability to fluorescently label lipids attached to trehalose by the Ag85 proteins should be useful in identifying other pathways that may use their transesterification activity and in helping clarify this poorly understood area of biochemistry.

Most notably, these assays have informed the design of a fluorescent probe that selectively labels *M. tuberculosis* in infected macrophages. Prior imaging work with *M. tuberculosis* in infected macrophages has used several strategies[41,42], but none allow for nontoxic imaging of bacteria *in vivo*. Bacteria can be labeled with Texas Red through oxidation with sodium periodate before infection. However, these harsh labeling conditions are nonselective and would be expected to oxidize carbohydrates that may be structurally important as well as peripherally associated glycolipids that may be important for specific virulence attributes[41]. Fluorescently labeled vancomycin has been elegantly used to track the cell division patterns of *M. smegmatis* and *M. bovis* BCG[42], but its toxicity toward *M. tuberculosis*[43] may affect experimental results. Antibodies can be used to label *M. tuberculosis* upon fixation and for enzyme-linked immunosorbant assays (ELISA)[44] but are not useful for live imaging. FITC-trehalose shows no significant inhibition of *M. tuberculosis* growth, which suggests that it does not perturb natural bacterial functions, thereby allowing imaging of healthy, viable bacteria. FITC-trehalose is also selective for *M. tuberculosis* and readily penetrates macrophages. Unlike other possible probes, its mode of action involves the activity of an enzyme unique to this genus of organisms. Given the highly conserved nature of the Ag85 proteins[45] in mycobacteria (and the complete absence of trehalose in mammalian biology), it is likely this probe would label nontuberculous mycobacteria as well as other members of the tuberculosis complex.

Our understanding of the macrophage infection process is incomplete[46], so the ability to follow viable *M. tuberculosis* during infection shown here could prove extremely useful as a means to further understand the bacterial transit to the phagosome as well as other

intracellular compartments. The colocalization studies between FITC-trehalose–labeled *M. tuberculosis* and various markers of phagosome maturation suggest that FITC-trehalose may preferentially label those bacteria that resist acidification and phagosome-lysosome fusion. An alternative hypothesis that we cannot rule out is that incorporation of FITC-trehalose into the membrane of a subset of bacilli alters the course of development of their phagosome, as has been seen with *Brucella pertusis* prelabeled with FITC before infection[47]. In our study FITC-trehalose is added after the infection has been established and is in low concentration relative to TDM; we expect the influence of the FITC-trehalose-DM to be slight. Other trehalose-tagged molecules, potentially labeled at different positions or with different tags on the trehalose scaffold, may also prove useful as additional *M. tuberculosis* probes. Future work with FITC-trehalose and related compounds will hopefully shed more light on its *in vivo* potential as a possible diagnostic tool to label *M. tuberculosis* in an infected host. Perhaps more notably, the broad substrate tolerance of the Ag85 proteins suggests the possibility of probes based on such analogs for a diverse panel of imaging modalities.

METHODS

Chemical synthesis

The synthesis of all reported compounds is described in the Supplementary Methods.

Mass spectrometry

Full details are described in the Supplementary Methods. Briefly, a 96-well plate was set up with each well containing TDH **27** and one of the screen compounds in 1 mM TEA buffer (pH = 7.2) at 37 °C. To each well was added by automated injection (with mixing) 20 μl of either Ag85A, Ag85B, Ag85C or buffer alone to give final concentrations of 500 μM of each substrate and 2 μM of Ag85. The samples were incubated at 37 °C for 2 h 40 min before injection of a 10-μl aliquot directly into the mass spectrometer. The resulting mass spectra were measured in ESI–continuum mode (150–1,000 Da), corrected for baseline subtraction and smoothed. The peak intensities for monohexanoylated product and remaining substrate **26** were measured and the product/substrate ratio calculated for each well.

^{14}C-trehalose uptake into infected macrophages

Mouse J774 macrophage cells were grown to confluence in Dulbecco's MEM containing 10% (v/v) FBS, 1 mmol l^{-1} L-glutamine and 1% (w/v) pyruvate (DMEM) in two 75-ml tissue culture flasks. The medium was exchanged, and one flask of cells was infected with a multiplicity of infection of 10 *M. tuberculosis*/macrophage of H37Rv bacteria. After 3 h, cells were washed with DMEM. Following 24 h incubation, the medium was exchanged, and ^{14}C-trehalose (10 μCi) was added to both infected and uninfected cultures. Cells were incubated with ^{14}C-trehalose for a further 24 h. Medium was removed and the supernatant clarified by centrifugation. Macrophages were gently washed with DMEM and lysed with PBS containing SDS 0.1% (w/v) (10 ml). Cells were further washed with PBS buffer (2 × 5 ml), and lysate was collected in falcon tubes and vortexed (1 min). The lysate was centrifuged at 3,600 r.p.m. for 20 min, and supernatant was poured off and collected for scintillation counting. The pelleted *M. tuberculosis* and controls were treated with four wash cycles of pelleting and resuspension (4 × 800 μl PBS with 0.1% (v/v) Tween 80). The pellet was resuspended in a minimal amount of PBS (200 μl) and added to scintillation fluid.

^{14}C- and FITC-trehalose lipid extractions

Lipid extractions from bacteria treated with ^{14}C-trehalose and ^{14}C-acetate are described fully in the Supplementary Methods. Briefly, ^{14}C-trehalose (10 μCi per tube) or ^{14}C-acetate

(30 μCi per tube) or dual ^{14}C-acetate (30 μCi per tube) and FITC-trehalose (to final concentration of 100 μM) were added to 15 ml H37Rv at optical density (OD_{650}) of 0.8. Cells were harvested and extracted into 2 ml (2:1 chloroform:methanol). The organic layer was removed and concentrated, and the residue was resuspended in 200 μl (80:20 chloroform:methanol), and 50 μl was spotted onto silica TLC plates, which were developed for 1 h (75:25:4 chloroform:methanol:water). Plates were scanned for fluorescence and exposed to a phosphor storage plate, which was scanned for radioactivity. See Supplementary Methods for isoniazid inhibition of mycolate synthesis and mycolate saponification.

FITC-trehalose and FITC-glucose uptake into *M. tuberculosis*

In vitro uptake experiments in *M. tuberculosis* and *H. influenza*e, *P. aeruginosa* and *S. aureus* are described in the Supplementary Methods.

Visualization of FITC-trehalose uptake into infected macrophages

In vitro: H37Rv-*M. tuberculosis* expressing RFP were grown in 7H9 medium to an OD = 0.25 at which point FITC-trehalose **9** in ethanol was added to a final concentration of 200 μM, and the culture was incubated with shaking for 24 h. The culture was then harvested and washed (3 × 1 ml PBS) by centrifugation and fixed in 5% (v/v) formalin (1:1 in PBS). The culture was pelleted and resuspended in PBS (200 μl) and mounted in suitable medium (Prolong GOLD, Invitrogen).

In vivo—Isolation of BMMs is described in the Supplementary Methods. J774 macrophages and BMMs were grown to confluence in supplemented DMEM on sterile coverslips. Cells treated with IFN-γ were exposed to 5 ng ml^{-1} mouse IFN-γ (Thermo RM200120) 18 h before infection. BMMs and J774s were infected with H37Rv *M. tuberculosis* (2–3 bacteria per macrophage). After 4 h of infection, macrophages were washed to remove free bacteria, and FITC-trehalose **9** was added in ethanol to a 200 μM final concentration. IFN-γ was replenished after washing. RFP-expressing BCG and H37Rv were infected using an identical procedure. Cells were fixed at different time points (24 h or 40 h) in 5% (v/v) formalin (1:1 in PBS), and coverslips were permeabilized, blocked and labeled with primary and secondary antibodies (see Supplementary Methods for full details), following standard immunocytochemical methods. Cells treated with just FITC-trehalose **9** were mounted in the same manner, in the absence of antibody. For cells labeled with DAPI, a 0.1 mg ml^{-1} stock solution of DAPI was made up in DMF, and cells were incubated with 1 μg ml^{-1} DAPI solution for 5 min immediately before mounting.

Microscopy

Images of stained cells were obtained by confocal microscopy (Leica SP5 equipped with AOBS and a white light laser, Leica Microsystems), using a ×63 oil immersion objective NA 1.4. Images were gathered sequentially and stacked when DAPI was used to label cells so as to minimize cross-talk between channels. Essential sequential Z sections of stained cells were also recorded for generation of stacked images through cells. A three-dimensional volume was constructed from sequential Z sections of cells assembled into such a volume in Imaris software (version 7.0.0, Bitplane AG). All collected images for analyses were deconvoluted by Huygens Essential software (Version 3.4, Scientific Volume Imaging BV). Percentage colocalization of material was calculated using the colocalization function in Imaris. Regions of interest for the poles and mid-sections were quantitated using the ‘marching cubes’ tool in Imaris to manually generate surfaces from which statistics were calculated for the regions of interest. *P* values were calculated from a one-tailed Student’s *t*-test. All statistics generated in GraphPad Prism (Version 5, GraphPad Software).

Other methods

Further experimental details for protein expression, minimum inhibitory concentration determination, ^{14}C-sugar uptake *in vitro* and polar labeling quantification of mycobacteria *in vitro* can be found in the Supplementary Methods.

Supplementary Material

Refer to Web version on PubMed Central for supplementary material.

Acknowledgments

We thank T. Claridge, B. Odell and T. Jackson for assistance with NMR spectra and C. Sparrow, J. McCullagh and R. Procter for their assistance with mass spectrometry. O. Schwartz, L. Koo, M. Gastinger, S. Becker and J. Kabat provided tremendous assistance on all imaging of *M. tuberculosis*. We thank the Colorado State "Tuberculosis Vaccine Testing and Research Materials" Contract (Colorado State University, Fort Collins) and G.J. Davies (University of York) for providing Ag85 and OtsA plasmids, respectively. We thank A. Sher (US National Institute of Allergy and Infectious Disease, US National Institutes of Health) for *M. bovis* BCG expressing DSRed1 and T. Oh (Yonsei University) for H37Rv carrying the mCherry-PMV261 plasmid. This study was supported (in part) by the Intramural Research Program of the US National Institutes of Health, the US National Institute of Allergy and Infectious Disease (C.E.B.), the Rhodes Trust (K.M.B.), a Marie Curie Intra European Fellowship (O.B.), the Engineering and Physical Sciences Research Council (Platform Grant to B.G.D.) and the Bill and Melinda Gates Foundation through the Tuberculosis Drug Accelerator Program (C.E.B., B.G.D.).

References

1. World Health Organization. Global Tuberculosis Control Report 2008. 2008.
2. Young DB. Confronting the scientific obstacles to global control of tuberculosis. J Clin Invest. 2008; 118:1255–1265. [PubMed: 18382738]
3. Daffé M, Etienne G. The capsule of *Mycobacterium tuberculosis* and its implications for pathogenicity. Tuber Lung Dis. 1999; 79:153–169. [PubMed: 10656114]
4. Murphy HN, et al. The OtsAB pathway is essential for trehalose biosynthesis in *Mycobacterium tuberculosis*. J Biol Chem. 2005; 280:14524–14529. [PubMed: 15703182]
5. Woodruff PJ, et al. Trehalose is required for growth of *Mycobacterium smegmatis*. J Biol Chem. 2004; 279:28835–28843. [PubMed: 15102847]
6. Hoffmann C, Leis A, Niederweis M, Plitzko JM, Engelhard H. Disclosure of the mycobacterial outer membrane: Cryo-electron tomography and vitreous sections reveal the lipid bilayer structure. Proc Natl Acad Sci USA. 2008; 105:3963–3967. [PubMed: 18316738]
7. Yamagami H, et al. Trehalose 6,6′-dimycolate (cord factor) of *Mycobacterium tuberculosis* induces foreign-body- and hypersensitivity-type granulomas in mice. Infect Immun. 2001; 69:810–815. [PubMed: 11159972]
8. Barry CE, Mdluli K. Drug sensitivity and environmental adaptation of mycobacterial cell wall components. Trends Microbiol. 1996; 4:275–281. [PubMed: 8829336]
9. Kilburn JO, Takayama KK, Armstrong EEL. Synthesis of trehalose dimycolate (cord factor) by a cell-free system of Mycobacterium smegmatis. Biochem Biophys Res Commun. 1982; 108:132–139. [PubMed: 7150277]
10. Fukui Y, Hirai T, Uchida T, Yoneda M. Extracellular proteins of tubercle bacilli. IV. Alpha and beta antigens as major extracellular protein products and as cellular components of a strain (H37Rv) of *Mycobacterium tuberculosis*. Biken J. 1965; 8:189–199. [PubMed: 4955992]
11. Jackson M, et al. Inactivation of the antigen 85C gene profoundly affects the mycolate content and alters the permeability of the *Mycobacterium tuberculosis* cell envelope. Mol Microbiol. 1999; 31:1573–1587. [PubMed: 10200974]
12. Puech V, Bayan N, Salim K, Leblon G, Daffe M. Characterization of the *in vivo* acceptors of the mycoloyl residues transferred by the corynebacterial PS1 and the related mycobacterial antigens 85. Mol Microbiol. 2000; 35:1026–1041. [PubMed: 10712685]

13. Ronning DR, et al. Crystal structure of the secreted form of antigen 85C reveals potential targets for mycobacterial drugs and vaccines. Nat Struct Biol. 2000; 7:141–146. [PubMed: 10655617]
14. Anderson DH, Harth G, Horwitz MA, Eisenberg D. An interfacial mechanism and a class of inhibitors inferred from two crystal structures of the *Mycobacterium tuberculosis* 30 kDa major secretory protein (Antigen 85B), a mycolyl transferase. J Mol Biol. 2001; 307:671–681. [PubMed: 11254389]
15. Ronning DR, Vissa V, Besra GS, Belisle JT, Sacchettini JC. *Mycobacterium tuberculosis* antigen 85A and 85C structures confirm binding orientation and conserved substrate specificity. J Biol Chem. 2004; 279:36771–36777. [PubMed: 15192106]
16. Belisle JT, et al. Role of the major antigen of *Mycobacterium tuberculosis* in cell wall biogenesis. Science. 1997; 276:1420–1422. [PubMed: 9162010]
17. Titgemeyer F, et al. A genomic view of sugar transport in *Mycobacterium smegmatis* and *Mycobacterium tuberculosis*. J Bacteriol. 2007; 189:5903–5915. [PubMed: 17557815]
18. Kalscheuer R, Weinricka B, Veeraraghavan U, Besra GS, Jacobs WR. Trehalose-recycling ABC transporter LpqY-SugA-SugB-SugC is essential for virulence of *Mycobacterium tuberculosis*. Proc Natl Acad Sci USA. 2010
19. Slayden RA, Barry CE. The genetics and biochemistry of isoniazid resistance in *Mycobacterium tuberculosis*. Microbes Infect. 2000; 2:659–669. [PubMed: 10884617]
20. Tufariello JM, Chan J, Flynn JL. Latent tuberculosis: mechanisms of host and bacillus that contribute to persistent infection. Lancet Infect Dis. 2003; 3:578–590. [PubMed: 12954564]
21. Demchenko AV. 1,2-cis O-Glycosylation: methods, strategies, principles. Curr Org Chem. 2003; 7:35–79.
22. Pratt MR, Leigh CD, Bertozzi CR. Formation of 11-alphaalpha-glycosidic bonds by intramolecular aglycone delivery. A convergent synthesis of trehalose. Org Lett. 2003; 5:3185–3188. [PubMed: 12943383]
23. Gobec S, et al. Design, synthesis, biochemical evaluation and antimycobacterial action of phosphonate inhibitors of antigen 85C, a crucial enzyme involved in biosynthesis of the mycobacterial cell wall. Eur J Med. 2007; 42:54–63.
24. Hui Y, Chang CW. Convenient divergent synthesis of a library of trehalosamine analogues. Org Lett. 2002; 4:2245–2248. [PubMed: 12074678]
25. Hadfield AF, Hough L, Richardson AC. The syntheses of 4,6-dideoxy-4,6-difluoro- and 4-deoxy-4-fluoro-alpha,alpha-trehalose. Carbohydr Res. 1979; 71:95–102.
26. Namme R, Hideyo TM, Ikegami TS. Development of ketoside-type analogues of trehalose by using stereoselective O-glycosidation of ketose. Eur J Org Chem. 2007; 2007:3758–3764.
27. Li X, Ohtake H, Takahashi H, Ikegami S. A facile synthesis of 1′-C-alkyl-α-disaccharides from 1-C-alkyl-hexopyranoses and methyl 1-C-methyl-hexopyranosides. Tetrahedron. 2001; 57:4297–4309.
28. Rodríguez MA, et al. Synthesis of 2-iodoglycals, glycals, and 1,1′-disaccharides from 2-deoxy-2-iodopyranoses under dehydrative glycosylation conditions. J Org Chem. 2007; 72:8998–9001. [PubMed: 17929873]
29. Giaever HM, Styrvold OB, Kaasen I, Strom AR. Biochemical and genetic characterization of osmoregulatory trehalose synthesis in *Escherichia coli*. J Bacteriol. 1988; 170:2841–2849. [PubMed: 3131312]
30. Yang M, et al. Probing the breadth of macrolide glycosyltransferases: in vitro remodeling of a polyketide antibiotic creates active bacterial uptake and enhances potency. J Am Chem Soc. 2005; 127:9336–9337. [PubMed: 15984838]
31. Converse SE, et al. MmpL8 is required for sulfolipid-1 biosynthesis and *Mycobacterium tuberculosis* virulence. Proc Natl Acad Sci USA. 2003; 100:6121–6126. [PubMed: 12724526]
32. Hatzios SK, et al. PapA3 is an acyltransferase required for polyacyltrehalose biosynthesis in *Mycobacterium tuberculosis*. J Biol Chem. 2009; 284:12745–12751. [PubMed: 19276083]
33. Abadie V, et al. Neutrophils rapidly migrate via lymphatics after *Mycobacterium bovis* BCG intradermal vaccination and shuttle live bacilli to the draining lymph nodes. Blood. 2005; 106:1843–1850. [PubMed: 15886329]

34. Spargo BJ, Crowe LM, Ioneda T, Beaman BL, Crowe JH. Cord factor (alpha,alpha-trehalose 6,6′-dimycolate) inhibits fusion between phospholipid vesicles. Proc Natl Acad Sci USA. 1991; 88:737–740. [PubMed: 1992465]
35. Indrigo J, Hunter RL Jr, Actor JK. Cord factor trehalose 6,6′-dimycolate (TDM) mediates trafficking events during mycobacterial infection of murine macrophages. Microbiology. 2003; 149:2049–2059. [PubMed: 12904545]
36. Fratti RA, Backer JM, Gruenberg J, Corvera S, Deretic V. Role of phosphatidylinositol 3-kinase and Rab5 effectors in phagosomal biogenesis and mycobacterial phagosome maturation arrest. J Cell Biol. 2001; 154:631–644. [PubMed: 11489920]
37. Kyei GB, et al. Rab14 is critical for maintenance of *Mycobacterium tuberculosis* phagosome maturation arrest. EMBO J. 2006; 25:5250–5259. [PubMed: 17082769]
38. Ullrich HJ, Beatty WL, Russell DG. Direct delivery of procathepsin D to phagosomes: implications for phagosome biogenesis and parasitism by *Mycobacterium*. Eur J Cell Biol. 1999; 78:739–748. [PubMed: 10569246]
39. Sturgill-Koszycki S, et al. Lack of acidification in *Mycobacterium* phagosomes produced by exclusion of the vesicular proton-ATPase. Science. 1994; 263:678–681. [PubMed: 8303277]
40. Matsunaga I, et al. Mycolyltransferase-mediated glycolipid exchange in mycobacteria. J Biol Chem. 2008; 283:28835–28841. [PubMed: 18703502]
41. Beatty WL, et al. Trafficking and release of mycobacterial lipids from infected macrophages. Traffic. 2000; 1:235–247. [PubMed: 11208107]
42. Thanky NR, Young DB, Robertson BD. Unusual features of the cell cycle in mycobacteria: polar-restricted growth and the snapping-model of cell division. Tuberculosis (Edinb). 2007; 87:231–236. [PubMed: 17287144]
43. Provvedi R, Boldrin F, Falciani F, Palu G, Manganelli R. Global transcriptional response to vancomycin in *Mycobacterium tuberculosis*. Microbiology-Sgm. 2009; 155:1093–1102.
44. Glatman-Freedman A, Martin JM, Riska PF, Bloom BR, Casadevall A. Monoclonal antibodies to surface antigens of *Mycobacterium tuberculosis* and their use in a modified enzyme-linked immunosorbent spot assay for detection of mycobacteria. J Clin Microbiol. 1996; 34:2795–2802. [PubMed: 8897185]
45. Cole ST, et al. Deciphering the biology of *Mycobacterium tuberculosis* from the complete genome sequence. Nature. 1998; 393:537–544. [PubMed: 9634230]
46. Schorey JS, Carroll MC, Brown EJ. A macrophage invasion mechanism of pathogenic mycobacteria. Science. 1997; 277:1091–1093. [PubMed: 9262476]
47. Weingart CL, et al. Fluorescent labels influence phagocytosis of *Bordetella pertussis* by human neutrophils. Infect Immun. 1999; 67:4264–4267. [PubMed: 10417202]
48. Anderson DH, et al. An interfacial mechanism and a class of inhibitors inferred from two crystal structures of the *Mycobacterium tuberculosis* 30 kDa major secretory protein (Antigen 85B), a mycolyl transferase. J Mol Biol. 2001; 307:671–681. [PubMed: 11254389]

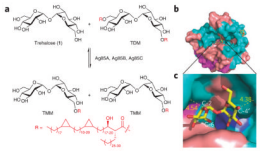

Figure 1. Ag85 structure and enzyme activity

(**a**) Ag85A, Ag85B and Ag85C catalyze transesterification of trehalose **1**, TDM and TMM. (**b**–**c**) The X-ray crystal structure of Ag85B suggests significant modification of trehalose substrates may be tolerated without altering binding contacts. Ag85B binds trehalose (yellow) (PDB ID: 1F0P)[48]. (**c**) The active site of Ag85B bound to trehalose. C-2 and C-4′ hydroxyls both point out of the active site. C-6 points into the hydrophobic tunnel (blue) that is thought to accommodate the long fatty acyl chains of the mycolic acids. Measurements to nearest residue are indicated in angstroms (PDB ID: 1F0P)[48]. Figure generated in PyMOL, Version 0.99rc6 (http://pymol.org/pymol).

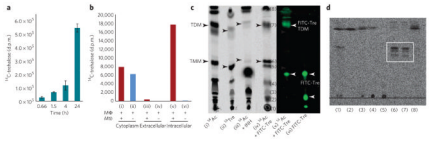

Figure 2. Trehalose is incorporated into *M. tuberculosis in vitro* and in macrophages

(**a**) Incorporation of ^{14}C-trehalose into *M. tuberculosis* culture over 24 h. (**b**) ^{14}C-trehalose was added either to *M. tuberculosis*–infected (i, iii, v), or to uninfected (ii, iv, vi) macrophages for 24 h. Supernatant was removed ("extracellular") and the macrophages were lysed and bacteria harvested by centrifugation to give a supernatant ("cytoplasm") and pellet ("intracellular") fraction. Radioactive trehalose is found in the cytoplasm yet accumulates in *M. tuberculosis* within infected macrophages. (**c**) ^{14}C-trehalose is incorporated into TMM and TDM in *M. tuberculosis*. Arrowheads show the migration position of authentic samples of TMM and TDM. In i, the culture was labeled for 24 h with ^{14}C-acetate to label fatty acids. In ii, the culture was labeled for 24 h with ^{14}C-trehalose. In iii, culture was treated with ^{14}C-acetate and INH to inhibit formation of TMM and TDM. ^{14}C-trehalose labels spots that comigrate with TMM and TDM. iv shows the radio TLC from dual labeling with FITC-trehalose and ^{14}C-acetate. v shows the fluorescence intensity in lane iv. vi shows a FITC-trehalose standard. (**d**) The glycolipids extracted from iv that comigrate with TDM and TMM contain mycolic acids; 1–8 correspond to individual spots from lane iv of **c** that were excised, saponified and run on a second TLC. The glycolipids in spots 6 and 7 contain lipids that comigrate with authentic mycolic acids and give the characteristic banding pattern of the three major mycolates. *M. tuberculosis*, *Mtb*; trehalose, Tre. Data reflect mean values ± s.d. for four experiments.

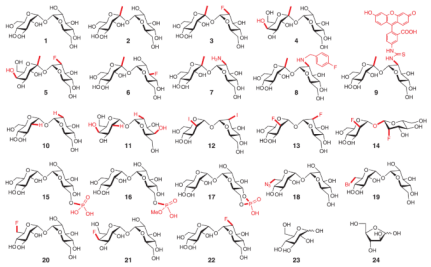

Figure 3. Trehalose library

Compound numbers match those in the green-amber-red screen (Table 1). Key modifications are highlighted in red. Syntheses and characterization of all compounds are described in the Supplementary Methods and Supplementary Results.

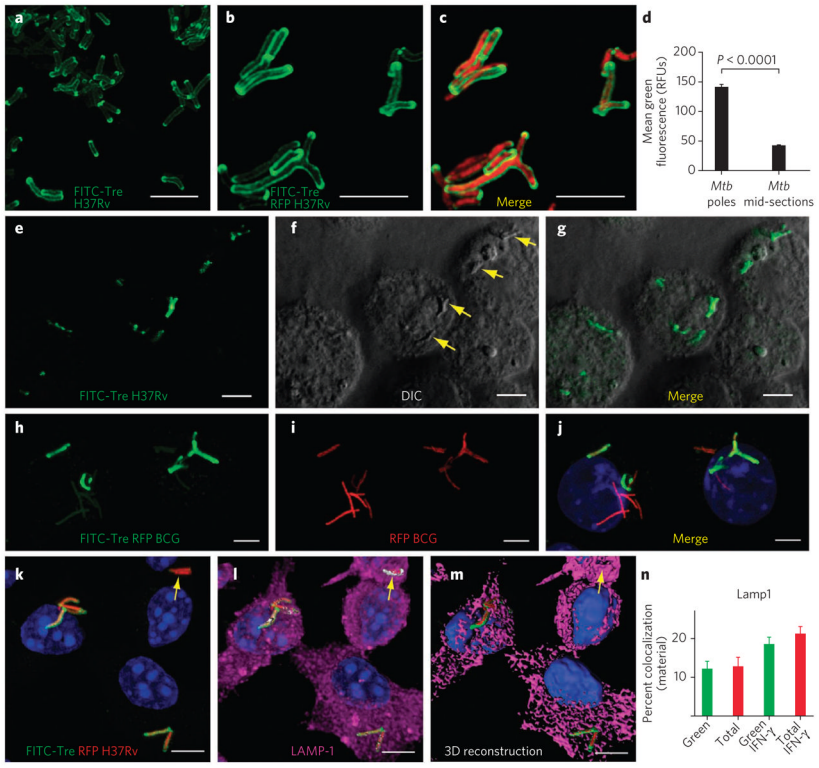

Figure 4. Labeling of individual bacilli *in vitro* and within infected macrophages

(**a**) H37Rv *M. tuberculosis* are labeled with FITC-trehalose and show signification accumulation of probe at the bacterial poles and membrane. (**b**) FITC-trehalose labeling of the RFP-expressing strain of H37Rv. (**c**) A merge of the FITC-trehalose and the RFP channels. (**d**) The mean fluorescence of poles and midsections of H37Rv *M. tuberculosis*, labeled with FITC-trehalose, are quantified and show statistically significant differential labeling. RFU, relative fluorescence units. (**e**–**g**) FITC-trehalose–labeled H37Rv-infected J774 macrophages. (**e**) FITC-trehalose–labeled H37Rv. In the DIC image **f**, the bacilli are indicated by arrows. The merged image (**g**) shows colocalization of FITC-trehalose and *M. tuberculosis*. (**h**–**j**) J774 BCG-RFP–infected macrophages. (**h**) Green labeling from FITC-trehalose. (**i**) Red labeling from RFP. (**j**) Merged images. (**k**–**n**) Triple labeling colocalization studies with RFP, FITC-trehalose and anti-LAMP antibody in H37Rv-RFP–infected BMMs activated with IFN-γ. Arrows indicate red bacteria that are not labeled with FITC-trehalose and that colocalize with LAMP-1. (**k**) The merged RFP and FITC images. (**l**) The labeling with anti-LAMP-1 (magenta) with colocalization indicated in white. (**m**) Three-dimensional reconstruction. (**n**) Quantitation of the colocalization between antibody signal and bacteria labeled with FITC-trehalose (green bars) or red bacteria (total population). *P* values for anti-LAMP-1: green versus green+IFN-γ (0.006), green versus total+IFN-γ (0.006), total versus green+IFN-γ (0.01), total versus total+ IFN-γ (0.001) and green+IFN-γ versus total+ IFN-γ (0.1). Error bars reflect s.e.m. for a minimum of three experiments. *P* values > 0.1 are not indicated. Scale bars, 5 μm. *M. tuberculosis*, *Mtb*; trehalose, Tre.

Nat Chem Biol. Author manuscript; available in PMC 2011 August 18.

Table 1

Green-amber-red screen of trehalose analogs

Compound	Ag85A	Ag85B	Ag85C	MIC	MIC_{50}
1	100	100	100	>200 μg ml^{-1}	>200 μg ml^{-1}
2	32	13	111	>200 μg ml^{-1}	>200 μg ml^{-1}
3	73	1415	102	>200 μg ml^{-1}	>200 μg ml^{-1}
4	12	7	57	>200 μg ml^{-1}	>200 μg ml^{-1}
5	19	13	64	>200 μg ml^{-1}	>200 μg ml^{-1}
6	7	8	76	>200 μg ml^{-1}	>200 μg ml^{-1}
7	47	56	91	>200 μg ml^{-1}	>200 μg ml^{-1}
8	25	14	81	>200 μg ml^{-1}	>200 μg ml^{-1}
9	**31**	**38**	**44**	**>200 mg ml^{-1}**	**>200 mg ml^{-1}**
10	50	16	129	>200 μg ml^{-1}	>200 μg ml^{-1}
11	1	4	1	100 μg ml^{-1}	ND
12	148	54	166	>200 μg ml^{-1}	>200 μg ml^{-1}
13	66	24	98	>200 μg ml^{-1}	>200 μg ml^{-1}
14	38	35	82	>200 μg ml^{-1}	>200 μg ml^{-1}
15	6	4	28	>200 μg ml^{-1}	>200 μg ml^{-1}
16	37	24	113	>200 μg ml^{-1}†	ND
17	18	17	94	>200 μg ml^{-1}	>200 μg ml^{-1}
18	37	13	49	>200 μg ml^{-1}†	135 μg ml^{-1}
19	102	92	99	200 μg ml^{-1}	134 μg ml^{-1}
20	149	412	91	200 μg ml^{-1}	75 μg ml^{-1}
21	229	162	191	100 μg ml^{-1}	50 μg ml^{-1}
22	115	156	274	>200 μg ml^{-1}	>200 μg ml^{-1}
23	18	19	45	>200 μg ml^{-1}	>200 μg ml^{-1}
24	6	28	8	>200 μg ml^{-1}	>200 μg ml^{-1}

Compound numbers correspond to those in Figure 3. FITC-trehalose entry 9 is bolded. Substrate response is expressed as percentage of natural substrate response: >75%, dark green; 25–75%, light green; 5–25%, amber; <5%, red. (Response = peak height (mono-Hex*)/peak height (trehalose*)). MIC, minimum inhibitory concentration; MIC_{50}, concentration causing 50% growth inhibition; ND, not determined.

† Has some growth inhibition at 200 μg ml.